PAPER

Check for updates

Conjugated polymer nanoparticles with tunable antibacterial photodynamic capability†

Anderson R. L. Caires, [ID] * Thalita H. N. Lima [ID] and Thais F. Abelha [ID] *

Conjugated polymers are versatile materials with promising applications as light-activated antibacterial agents. This work investigated the photoantimicrobial effect of conjugated polymer nanoparticles (CPNs) composed of poly(2.5-di(hexyloxy)cyanoterephthalylidene) (CN-PPV) prepared under different conditions *via* a nanoprecipitation method. The stabilization of CN-PPV CPNs with the surfactant polysorbate 20 (tween® 20) increased the CN-PPV product yields and resulted in the formation of nanoparticles of diminished size with slightly negative charge; which did not affect the cell viability of *S. aureus* and *E. coli* in the absence of light. Altering the ratio of the organic to aqueous phase from 1:10 to 2:10 (tetrahydrofuran – THF:water) led to the formation of CPNs of smaller size that presented increased photostability compared to that of 1:10 counterparts. All CPNs were capable of generating reactive oxygen species (ROS) under illumination (450 nm). In addition, CPNs produced with a 2:10 THF:H₂O ratio presented the highest photoantimicrobial activity against both Gram-positive (*S. aureus*) and Gram-negative (*E. coli*) bacteria. Overall, by changing the CPN preparation conditions, CPNs of the same conjugated polymer having remarkably different properties, including greater photostability and more effective microorganism inactivation following photoexcitation, can be generated.

Introduction

Bacteria are abundant prokaryote microorganisms that colonize virtually all habitats of the planet.[1,2] Amongst their great diversity, some strains cause diseases of varied severity and have become resistant to traditional antibiotic therapy, leading to a worldwide crisis of effective treatments.[3,4] The consequences of the antibiotic resistance crisis include the increased cost for health care systems, higher mortality rates and the compromise of surgical procedures that rely on antibiotic efficacy.[4,5] The increasing number of multidrug-resistant microorganisms is an ongoing problem that will continue worsening; thus there is an urgent need for the development of new effective treatments against pathogenic bacteria and their antibiotic-resistant strains.[3,4,6] Besides the search for new antibiotics, photosensitizer (PS) agents, which are capable of tackling bacteria through the generation of reactive oxygen species (ROS) by light stimulation, have been used as an alternative and successful treatment.[7] Although photodynamic therapy (PDT) was discovered over a hundred years ago, there is a recent interest in the development of new PSs with improved performance.[8,9]

Federal University of Mato Grosso do Sul, Institute of Physics, Mato Grosso do Sul, Campo Grande 79070-900, Brazil. E-mail: thais.abelha@ufms.br, anderson.caires@ufms.br

† Electronic supplementary information (ESI) available. See DOI: https://doi.org/10.1039/d2ma00970f

Conjugated polymers are versatile organic materials that have been broadly explored for biomedical applications.[2,10–12] There has been a growing interest in applying their useful physicochemical properties for bacterial photothermal and photodynamic therapies, with promising results.[2] For example, conjugated polymer nanoparticles (CPNs) presented light-activated cytotoxicity against both bacteria planktonic solutions and biofilms with good selectivity and biocompatibility *in vivo*.[2] In addition, the conjugated polymer chemical structure can be refined to achieve greater ROS/heat generation capabilities and to enhance water dispersibility, while enabling greater targetability against microorganisms.[2] The commercially available conjugated polymer poly(2.5-di(hexyloxy)cyanoterephthalylidene) (CN-PPV) has been successfully explored for fluorescence bioimaging[13] and has potential applications as a photosensitizer[14] due to its useful optical features. The optical properties of such materials are highly dependent not only on the environment in which they are dispersed (such as solvent polarity and nanoparticle forming agent composition), but also on the nanoparticle preparation settings.[10,11,15,16] For example, nanoparticles of CN-PPV embedded into the poly(ethylene glycol) methyl ether-*block*-poly(lactide-*co*-glycolide) (PEG-PLGA) polymer exhibited redshifted emission compared to the conjugated polymer in tetrahydrofuran (THF) and variable fluorescence quantum yield in water (35–55% CN-PPV) depending on the manufacturing settings (microfluidics or bulk method).[15]

The influence of the method of nanoparticle preparation on the performance of conjugated polymers as PS agents is still
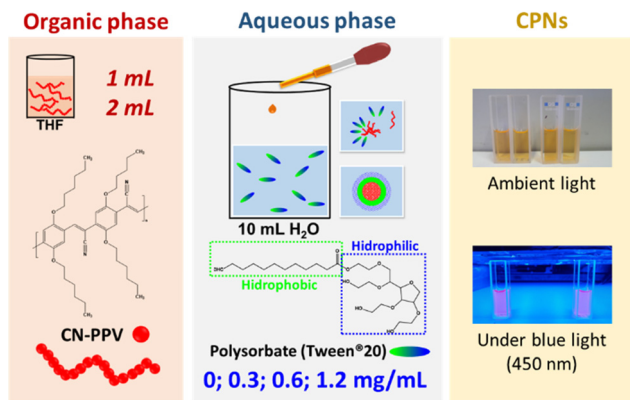
Fig. 1 Illustration of CPN preparation conditions and representative images of the nanoparticles under ambient light and blue light illumination.

open to investigation. CN-PPV present tunable optical properties[15] that might be useful for inactivating bacteria, but such characteristics have not been explored yet in this scenario. Therefore, the study of the influence of preparation conditions on the CPN photoinactivation capability would enable the screening for optimized conditions to produce high-performance CPNs against bacteria. In this work, CN-PPV CPNs were prepared by varying the ratio of organic (CN-PPV/THF) and aqueous phases and the concentrations of polysorbate 20 in water (Fig. 1). The chosen surfactant (Tween® 20) is a broadly used colloid stabilizing agent and is present in many commercialized pharmaceutical formulations.[17] Regarding the choice of microorganisms, *Staphylococcus aureus* and *Escherichia coli* have been used by most literature studies that evaluated the anti-bacterial performance of conjugated polymers; accordingly, they are a good model of both Gram-positive and negative bacteria, enabling comparison with the literature record.[2] *Staphylococcus aureus* is a Gram-positive bacteria that causes complicated skin infections and has developed resistant strains, especially to methicillin; its incidence is increasing, causing life-threatening illnesses (*e.g.*, necrotizing pneumonia) that are not responsive to conventional treatments.[18] It also thrives within the human flora without being harmful to healthy individuals, causing easy spread, which has already triggered a pandemic worldwide due to the lack of available treatment.[18] As to the Gram-negative *Escherichia coli*, it is one of the most abundant microorganisms in the healthy human gut flora, but when pathogenic strains thrive, they may cause diarrhoea and extraintestinal conditions like urinary tract infections and sepsis/meningitis.[19]

Experimental

Nanoparticle preparation

CPNs of the commercially available conjugated polymer poly(2.5-di(hexyloxy)cyanoterephthalylidene) (CN-PPV) (Sigma-Aldrich Corporation, USA) were prepared by an adapted nano-precipitation method.[20] Briefly, an organic solution of CN-PPV in tetrahydrofuran (THF) was added dropwise to 10 mL of water containing varied concentrations (0; 0.3; 0.6 and 1.2 mg mL^{-1})

of polysorbate 20 (tween® 20, Quimesp Química Ltda, Brazil). The CPNs were prepared with THF:H$_2$O ratios of 1:10 and 2:10. After stirring overnight, the water lost due to evaporation was replaced and the CN-PPV content (product yield) of each formulation was characterized as previously described,[15] as the conjugated polymer attachment to the magnetic stirrer and vial walls was visually noticeable. The CN-PPV theoretical concentration in the end product was 45 µg mL^{-1}.

Instrumentation

Dynamic light scattering (DLS) (Zetasizer NanoZS, Malvern Instruments Ltd, UK) was used to characterize the hydrodynamic diameters (expressed as *Z*-average values obtained from the intensity distribution of particle size) and zeta potential of CPNs at 25 °C. CPNs stabilized with surfactants were characterized at concentrations below and above tween® 20 critical micellar concentration (CMC, 60 µg mL^{-1}) shortly after dilution. For zeta potential analysis, NaCl was added to CPN samples at a final working concentration of 6 mM. Absorbance spectra were obtained between 250 and 800 nm using a UV-vis absorption spectrometer (Lambda 265, PerkinElmer, USA). Fluorescence measurements were performed at room temperature with a spectrofluorimeter (Scinco FS-2, Seoul, Korea) in a right-angle geometry with the aid of a quartz cuvette with four polished faces and 1 cm optical path length. The CPN fluorescence spectra were collected in the 470 to 800 nm range with 460 nm excitation. To irradiate samples, a previously described light emitting diode (LED) device was used.[21] To assess the photostability of CPNs under blue light (450 nm) irradiation, absorbance and fluorescence spectra of the samples containing 20 µg mL^{-1} CN-PPV were measured prior to illumination (time 0) and after 30 and 60 minutes of light exposure at 27 mW cm^{-2}. Fourier transform infrared spectroscopy (FTIR) was used to further assess the structural changes induced by light exposure. For FTIR characterization, CN-PPV powder was used as provided by the manufacturer and CPNs prepared at 1:10 and 2:10 THF:H$_2$O ratios and with 0 and 1.2 mg mL^{-1} tween® 20 were dried on silicon wafers prior to light exposure and after 30 and 60 minutes of light irradiation. FTIR spectra were collected by using a spectrometer (Spectrum 100, PerkinElmer, USA) equipped with an ATR accessory. Acellular reactive oxygen species (ROS) produced by CNPs under blue light (450 nm) illumination at 27 mW cm^{-2} was assessed using a dihydroethidium (DHE) probe by monitoring the fluorescent oxidized products originated under illumination due to the interaction between the photoproduced ROS and DHE. Absorbance and fluorescence emission ($\lambda_{ex.}$: 500 nm) spectra of CPNs at 5 µg mL^{-1} CN-PPV (2 mL) were assessed prior to the addition of 4 µL of DHE stock (5 mM) and at time 0 after DHE addition. In sequence, the spectra were acquired at 1-minute intervals for 10 min in the dark and then blue light was turned on and the spectra were collected every minute for 10 minutes under continuous illumination. Due to the intrinsic fluorescence of CN-PPV, absorbance ($\lambda_{470\,nm}$) and fluorescence ($\lambda_{580\,nm}$) measurements were investigated to characterize the formation of DHE oxidized products and the data

were normalized at time 0 after DHE addition to CPN samples. GraphPad Prism (version 5.00 for Windows, GraphPad Software, San Diego California, USA) was used to perform statistical analysis (One-way ANOVA with Tukey *post hoc* test).

Microbiological assays

Staphylococcus aureus (strain 25923) and *Escherichia coli* (strain 25922) were acquired from the American Type Culture Collection (ATCC). The bacterial strains were grown in sterilized brain heart infusion broth (BHIB, KASVI, Brazil) and, for biological assays, diluted in sterile phosphate buffer saline (PBS) to adjust the bacterial concentration to the 0.5 McFarland scale (1.5×10^8 bacteria mL^{-1}, Probac do Brasil, Brazil). The cell metabolic activity was assessed using (3-(4,5-dimethylthiazol-2-yl)-2,5-diphenyl-tetrazolium bromide) (MTT) tetrazolium assay.[22] Briefly, bacteria receiving CPN treatments (5 µg mL^{-1} CN-PPV working concentration) and controls (PBS and tween® 20 solution at 0.2 mg mL^{-1}) were kept in the dark for 30 min. Then, 100 µL samples were transferred to a 96-well plate in triplicate and irradiated (450 nm at 27 mW cm^{-2}) for 1 h. In sequence, 100 µL of the samples kept in the dark were transferred in triplicate to a 96-well plate and 10 µL of MTT stock solution (5 mg mL^{-1}) was added to each well and the plate was incubated at 37 °C for 4h protecting from light. The formazan crystals were solubilized with isopropanol and the prevalence of its purple colour was visually inspected. The colony assay was performed similarly, except that after light exposure, the samples kept in the dark and under radiation were diluted gradually with PBS (1:200, 1:200 and 1:37 fold) and 100 µL was transferred and spread onto agar plates (90 × 15 mm) in duplicate. After 18 h of incubation at 37 °C, the bacterial colonies present on the agar plates were counted and the colony-forming units (CFU) per mL was calculated taking into account the sample dilution factor and the volume transferred to the plates.

Results and discussion

CN-PPV nanoparticles were generated with variable preparation settings that influenced the final product yield (Fig. 2). Although CN-PPV can self-assemble into nanoparticles in water by forming nanoaggregates due to the folding and collapsing of their hydrophobic chains,[13,15] increasing tween® 20 concentration in the
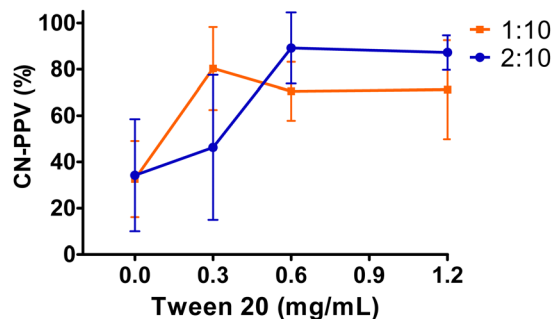
aqueous phase greatly contributed to high CN-PPV yields in the end product, whereas in the absence of tween® 20, the mean product yields were below 35%. In addition, a THF:H$_2$O ratio of 2:10 led to higher mean product yields at higher tween® 20 concentrations. Overall, increasing the surfactant concentration and the THF:H$_2$O ratio improved the CN-PPV product yield and led to lower batch variability. The mean CN-PPV yield of CPNs prepared with 0.6 and 1.2 mg mL^{-1} tween® 20 was comparable with that of CPNs of the same conjugated polymer prepared with a bulk nanoprecipitation method, but stabilized with PEG-PLGA.[15]

CPNs prepared in water presented significantly ($p \leq 0.05$) larger mean diameters than the counterparts generated with the same THF:H$_2$O ratio, but containing tween® 20 (Fig. 3a). In addition, CPNs prepared with the 2:10 THF:H$_2$O ratio presented significantly ($p \leq 0.05$) smaller hydrodynamic diameters (< 130 nm) compared to the ones generated with the 1:10 ratio (<220 nm), except for the ones containing 1.2 mg mL^{-1} tween® 20. The increasing content of the surfactant in the aqueous phase showed a significant ($p \leq 0.05$) influence only on the nanoparticle size for CPNs prepared at the 1:10 THF:H$_2$O ratio, as it led to a CPN size reduction similar to nanoparticles prepared with the 2:10 THF:H$_2$O ratio (*ca.* 118 nm for 1.2 mg mL^{-1} tween® 20). Overall, nanoparticles with smaller sizes were prepared with the 2:10 THF:H$_2$O ratio, regardless of the surfactant concentration, and with the 1:10 THF:H$_2$O ratio with 1.2 mg mL^{-1} tween® 20. The polydispersity indexes of all CPNs were typically between 0.10–0.25, regardless of the production settings, and they slightly increased when CPNs were diluted below the CMC of tween® 20. CPNs prepared with tween® 20 presented a mild negative

Fig. 2 CN-PPV product yield of CPNs prepared with variable preparation settings: 1:10 and 2:10 THF:H$_2$O ratios and increasing surfactant concentration (0; 0.3; 0.6 and 1.2 mg mL^{-1}).
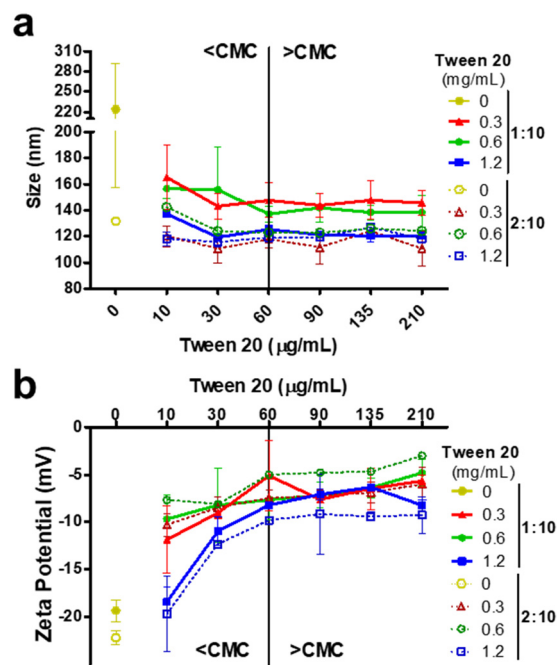
Fig. 3 Hydrodynamic diameters (a) and zeta potential (b) of CPNs characterized above and below the CMC of tween® 20. The CPNs prepared without tween® 20 are denoted as 0 mg mL^{-1}.
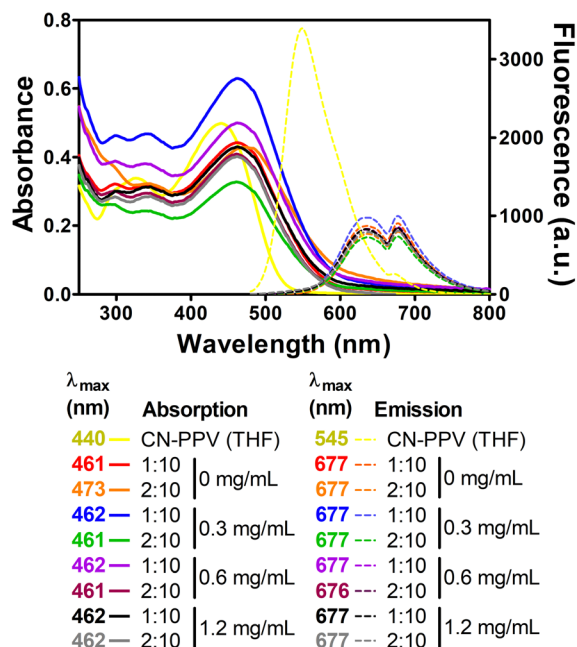
Fig. 4 Absorption and fluorescence intensity spectra of CNPs at 20 μg mL⁻¹ CN-PPV.

charge, while the zeta potential of bare CN-PPV nanoparticles was more electronegative (Fig. 3b), in agreement with the previous report.[15] It was noteworthy that CPNs diluted below the CMC of tween® 20 presented more electronegative zeta potential values, which we attribute to micelle destabilization and exposure of the electronegative cyan groups of CN-PPV.

It is known that the optical properties of conjugated polymers are highly dependent on their chain conformation, which is influenced by nanoparticle preparation conditions.[10,15,16] Under microfluidic conditions, different THF : H₂O ratios generated CN-PPV CPNs with distinctive optical properties,[15] while in this work, all CPNs presented similar absorption and fluorescence emission spectra, independent of the preparation settings (Fig. 4). Compared to CN-PPV solution in THF, the maximum absorption of CPNs was approximately 20 nm red-shifted, while their maximum fluorescence emission wavelength presented a red-shift of approximately 132 nm, which is greater than that previously reported for CN-PPV nanoparticles prepared via a similar bulk method.[15] Importantly, the red-shifted emission leads to a desirable large Stokes shift (decreasing the probability of self-absorption) and near-infrared emission that is more suitable for biomedical applications. Noteworthily, a distinct spectral shape of fluorescence emission compared to that of the conjugated polymer in organic solvent was observed. This was
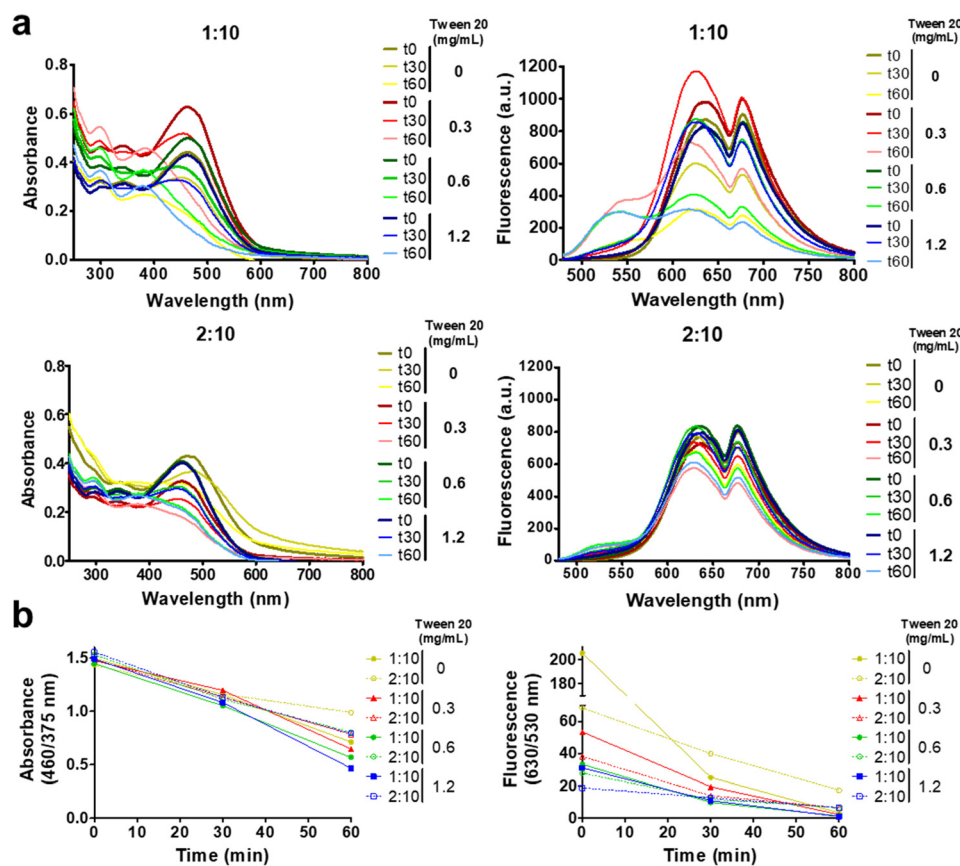

Fig. 5 Photostability of CPNs before and after exposure to light (450 nm). Absorption and fluorescence intensity spectra of CPNs at 20 μg mL⁻¹ CN-PPV prior to light exposure (t0) and after 30 and 60 minutes of light irradiation (a). Ratio of absorbance (at 460 and 375 nm) and fluorescence (630 and 530 nm) (b).

observed as a dual-band emission due to the self-arrangement and interactions of the confined CN-PPV polymers within the nanoparticle structure. The dual-band characteristic indicates the existence of aggregated states in the confined nanoparticle architecture, allowing emission originating from intrachain and interchain interactions, which may explain the observed red shift and dual-band emission feature of CN-PPV CNPs.[23–30]

In order to study the CPN photostability under 450 nm light irradiation, the absorption and fluorescence emission spectra of nanoparticle solutions with the same CN-PPV content were monitored prior to illumination and after continuous irradiation for 30 and 60 minutes. Fig. 5a and Fig. S1 (ESI†) reveal that regardless of the tween® 20 concentrations, after 30 minutes of irradiation there was a decrease in absorbance intensity at 460 nm and an increase in absorption at 290 nm, which continued to change under 60 minute light exposure, reaching the maximum absorbance intensity at 290 nm with a second peak at 375 nm. The fluorescence emission spectra showed a blue-shifted spectra with increasing light exposure time, resulting in diminished intensities and the appearance of a shoulder at ~530 nm after 60 minutes of light irradiation. It is noteworthy that CPNs prepared with different THF:H$_2$O ratios showed remarkably different susceptibility to light irradiation, with 2:10 (THF:H$_2$O) nanoparticles presenting a lower extent of spectral alterations than 1:10 CPNs, independent of the concentration of tween® 20 (Fig. 5b). We ascribed the spectroscopic alterations to the photodegradation of CN-PPV. Hence, to further characterize the effect of light exposure, the size, zeta potential and FTIR of CPNs prepared with 1:10 and 2:10 THF:H$_2$O ratios and with no stabilizing agent and with 1.2 mg mL^{-1} tween® 20 were investigated. While the FTIR analysis did not reveal any functional group alteration with increasing irradiation times (Fig. S2, ESI†), the DLS analysis of photostable samples (Fig. S2, ESI†) showed that both 1:10 and 2:10 CPNs without tween® presented a decrease in electronegativity from approximately −20 mV to −5 mM, suggesting an alteration in the sample composition after illumination.

The light-activated ROS generation capability of CN-PPV CPNs was assessed using the DHE probe.[31] Although DHE is non-fluorescent, ethidium is generated in the presence of ROS and its fluorescence emission (530 to 750 nm range) can be monitored.[32] Due to the overlap between the intrinsic spectra of CN-PPV CPNs and ethidium, the ROS production was determined from the relative intensity variation as a function of the time after normalizing the fluorescence and absorption spectra at the initial time (i.e., after the addition of DHE to CPN samples at time 0). Fig. 6a and b reveals that upon light exposure there is a sharp increase in fluorescence and absorbance intensities for all CPN samples. Overall, the CPNs prepared with the 2:10 THF:H$_2$O ratio presented higher intensity values than the corresponding 1:10 formulations.

The light-activated antimicrobial activity of CN-PPV CPNs was evaluated in Gram-positive (S. aureus) and Gram-negative (E. coli) bacteria, both widely used to study the photoinactivation capability of conjugated polymers.[2] MTT tetrazolium assay was used to evaluate the influence of treatments and controls
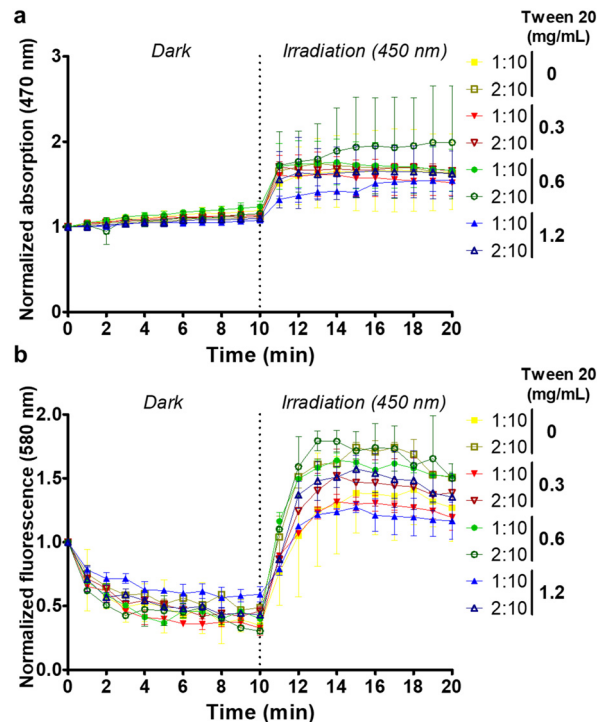
Fig. 6 ROS generation capability of CPNs exposed to light (450 nm) assessed by fluorescence (a) and absorbance (b) measurements of DHE probe oxidized products (CPNs at 5 μg mL^{-1} CN-PPV and DHE at 10 μM).

on the cell metabolic activity. Fig. S3 (ESI†) shows a reduction in the metabolic activity of both Gram-positive and Gram-negative bacteria exposed to light in the presence of CN-PPV nanoparticles, observed from lower staining intensity due to the reduced metabolism of MTT to the purple coloured tetrazolium.[22,33] It is noteworthy that the nanoparticles prepared without a stabilizing agent reduced the metabolic activity of bacterial strains kept in the dark, while the nanoparticles prepared with tween® 20 were more compatible in the absence of irradiation and were activated only in the presence of light, which is a desirable characteristic for new materials investigated for photodynamic therapy.

To characterize the bacterial photoinactivation of CN-PPV nanoparticles, the CPNs prepared at 1:10 and 2:10 (THF:H$_2$O) ratios, without the surfactant and with the highest concentration of tween® 20 (1.2 mg mL^{-1}) were selected for the colony assay. It was observed that S. aureus and E. coli presented different susceptibility to the different irradiated treatments, with the Gram-negative bacteria showing a lower extent of reduction compared to the Gram-positive strain (Fig. 7 and Fig. S3, ESI†). The log$_{10}$ CFU reduction of bacteria exposed to CPNs under light illumination was larger than that of the control, irrespective of the nanoparticle preparation conditions (Fig. 7c). It is noteworthy that the CPNs prepared at the 2:10 ratio (THF:H$_2$O) and without a stabilizing agent presented the greatest light-induced bacteria inactivation with approximately 3 and 5.5 Log$_{10}$ CFU reduction for E. coli and S. aureus, respectively. In fact, S. aureus was more susceptible to CPNs prepared at the 2:10 ratio (THF:H$_2$O), independent of the
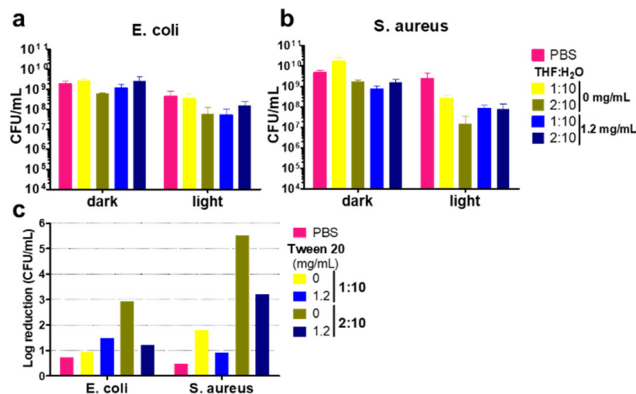
Fig. 7 Charts representing mean CFU mL^{-1} of *S. aureus* (a) and *E. coli* (b). Log$_{10}$ reduction calculated from mean values of bacterial strains kept in dark and exposed to light (c).

presence of tween® 20. This could be related to the greater photostability of CPNs prepared with the 2:10 ratio setting. In spite of the fact that the majority of novel photosensitizers are designed with a positive charge to facilitate their interaction with the bacterial anionic cell wall,[2] electronegative CN-PPV nanoparticles were capable of inducing cytotoxicity triggered by light to both Gram-negative and Gram-positive bacteria.

Conclusions

In this work, we report the light-activated antibacterial capability of CN-PPV nanoparticles prepared with variable settings. We show that increasing concentrations of polysorbate 20 (tween® 20) in an aqueous phase led to the formation of smaller CPNs with higher CN-PPV yields in the final product and that the use of the 2:10 THF:H$_2$O ratio led to the formation of CPNs of smaller sizes compared to their 1:10 counterparts. CPNs stabilized with tween® 20 presented mild negative charge, while the ones prepared without the surfactant were more electronegative. The preparation conditions studied did not affect the absorbance and emission spectra profile of CPNs, which were red-shifted and presented two emission peaks compared to CN-PPV in THF. All CPNs were capable of generating ROS under blue light irradiation, affecting the cell metabolic activity and photoinactivating both Gram-positive and Gram-negative bacteria. It was noteworthy that while CPNs presented similar absorbance and emission spectra, changing the organic and aqueous ratio from 1:10 to 2:10 led to the formation of nanoparticles with diminished size, improved photostability and more efficiency toward bacterial inactivation. The most successful antibacterial photodynamic agent was prepared without tween® 20 and with a 2:10 THF:H$_2$O ratio; however such CPNs presented lower CN-PPV yield and affected the cell metabolic activity in the dark. Nonetheless, CPNs containing tween® 20 were capable of 3 log$_{10}$ CFU reduction, while being inert in the dark. Overall, this work showed that CPNs prepared with commercially available products could show enhanced antibacterial performance by altering the nanoparticle production setting, without requiring complicated synthesis of novel materials.

Author contributions

TFA was responsible for the conceptualization, data curation, formal analysis, funding acquisition, investigation, methodology, project administration, supervision and writing (original draft). ARLC contributed with the conceptualization, funding acquisition, investigation, methodology and writing (review and editing). THNL participated in data curation, investigation, methodology and writing (review and editing).

Conflicts of interest

There are no conflicts to declare.

Acknowledgements

References

1 L. A. Cole, *Biology of Life*, Elsevier, 2016, pp. 93–99.
2 T. Fedatto Abelha and A. Rodrigues Lima Caires, *Adv. NanoBiomed. Res.*, 2021, **1**, 2100012.
3 World Health Organisation, Prioritization of pathogens to guide discovery, research and development of new antibiotics for drug resistant bacterial infections, including tuberculosis, Geneva, Switzerland, 2017.
4 K. Bush, P. Courvalin, G. Dantas, J. Davies, B. Eisenstein, P. Huovinen, G. A. Jacoby, R. Kishony, B. N. Kreiswirth, E. Kutter, S. A. Lerner, S. Levy, K. Lewis, O. Lomovskaya, J. H. Miller, S. Mobashery, L. J. V. Piddock, S. Projan, C. M. Thomas, A. Tomasz, P. M. Tulkens, T. R. Walsh, J. D. Watson, J. Witkowski, W. Witte, G. Wright, P. Yeh and H. I. Zgurskaya, *Nat. Rev. Microbiol.*, 2011, **9**, 894–896.
5 J. O'neill, Tackling drug-resistantinfections globally: Final-report and recommendations, 2016.
6 World Health Organisation, Global Action Plan on Antimicrobial Resistance, 2015.
7 Y. Liu, R. Qin, S. A. J. Zaat, E. Breukink and M. Heger, *J. Clin. Transl. Res.*, 2015, **1**, 140–167.
8 H. Hönigsmann, *Photochem. Photobiol. Sci.*, 2013, **12**, 16–21.
9 S. Liu, G. Feng, B. Z. Tang and B. Liu, *Chem. Sci.*, 2021, **12**, 6488–6506.

10 T. F. Abelha, C. A. Dreiss, M. A. Green and L. A. Dailey, *J. Mater. Chem. B*, 2020, **8**, 592–606.

11 T. F. Abelha, P. R. Neumann, J. Holthof, C. A. Dreiss, C. Alexander, M. Green and L. A. Dailey, *J. Mater. Chem. B*, 2019, **7**, 5115–5124.

12 R. A. Khanbeigi, Z. Hashim, T. F. Abelha, S. Pitchford, H. Collins, M. Green and L. A. Dailey, *J. Mater. Chem. B*, 2015, **3**, 2463–2471.

13 E. Kemal, T. F. Abelha, L. Urbano, R. Peters, D. M. Owen, P. Howes, M. Green and L. A. Dailey, *RSC Adv.*, 2017, **7**, 15255–15264.

14 P. L. C. Feyen, B. F. E. Matarèse, L. Urbano, T. F. Abelha, H. Rahmoune, M. Green, L. A. Dailey, J. C. de Mello and F. Benfenati, *Front. Bioeng. Biotechnol.*, 2022, **10**, 932877.

15 T. F. Abelha, T. W. Phillips, J. H. Bannock, A. M. Nightingale, C. A. Dreiss, E. Kemal, L. Urbano, J. C. de Mello, M. A. Green and L. A. Dailey, *Nanoscale*, 2017, **9**, 2009–2019.

16 T. F. Abelha, J. Calvo-Castro, S. M. Lima, J. R. Silva, L. H. da Cunha Andrade, J. C. de Mello, C. A. Dreiss, M. Green and L. A. Dailey, *ACS Appl. Polym. Mater.*, 2022, **4**, 6219–6228.

17 A. Martos, W. Koch, W. Jiskoot, K. Wuchner, G. Winter, W. Friess and A. Hawe, *J. Pharm. Sci.*, 2017, **106**, 1722–1735.

18 H. F. Chambers and F. R. DeLeo, *Nat. Rev. Microbiol.*, 2009, **7**, 629–641.

19 J. B. Kaper, J. P. Nataro and H. L. T. Mobley, *Nat. Rev. Microbiol.*, 2004, **2**, 123–140.

20 L. Urbano, L. Clifton, H. K. Ku, H. Kendall-Troughton, K. A. Vandera, B. F. E. Matarese, T. Abelha, P. Li, T. Desai, C. A. Dreiss, R. D. Barker, M. A. Green, L. A. Dailey and R. D. Harvey, *Langmuir*, 2018, **34**, 6125–6137.

21 C. M. Silva, A. R. Lima, T. F. Abelha, T. H. N. Lima, C. S. A. Caires, T. V. Acunha, E. J. Arruda, S. L. Oliveira, B. A. Iglesias and A. R. L. Caires, *J. Photochem. Photobiol., B*, 2021, **224**, 112323.

22 E. Grela, J. Kozłowska and A. Grabowiecka, *Acta Histochem.*, 2018, **120**, 303–311.

23 C. Wu, B. Bull, C. Szymanski, K. Christensen and J. McNeill, *ACS Nano*, 2008, **2**, 2415–2423.

24 B. J. Schwartz, *Annu. Rev. Phys. Chem.*, 2003, **54**, 141–172.

25 L. E. Ibarra, S. R. Martínez, R. A. Ponzio and R. E. Palacios, *Advances in Photodynamic Therapy Research*, Nova Science Publishers, 2020, pp. 65–92.

26 D. A. Vanden Bout, W.-T. Yip, D. Hu, D.-K. Fu, T. M. Swager and P. F. Barbara, *Science*, 1997, **277**, 1074–1077.

27 J. Kim, *Pure Appl. Chem.*, 2002, **74**, 2031–2044.

28 F. C. Spano and C. Silva, *Annu. Rev. Phys. Chem.*, 2014, **65**, 477–500.

29 M. E. Ziffer, S. B. Jo, Y. Liu, H. Zhong, J. C. Mohammed, J. S. Harrison, A. K.-Y. Jen and D. S. Ginger, *J. Phys. Chem. C*, 2018, **122**, 18860–18869.

30 K. Li and B. Liu, *J. Mater. Chem.*, 2012, **22**, 1257–1264.

31 R. R. Nazarewicz, A. Bikineyeva and S. I. Dikalov, *J. Biomol. Screen.*, 2013, **18**, 498–503.

32 D. P. Pedruzzi, L. O. Araujo, W. F. Falco, G. Machado, G. A. Casagrande, I. Colbeck, T. Lawson, S. L. Oliveira and A. R. L. Caires, *NanoImpact*, 2020, **19**, 100246.

33 T. Mosmann, *J. Immunol. Methods*, 1983, **65**, 55–63.